Shock Waves (2007) 17:95–102
DOI 10.1007/s00193-007-0093-y

ORIGINAL ARTICLE

Behavior of detonation propagation in mixtures with concentration gradients

K. Ishii · M. Kojima

Received: 7 July 2006 / Revised: 25 May 2007 / Accepted: 30 May 2007 / Published online: 28 July 2007

Abstract Behavior of detonation waves in mixtures with concentration gradients normal to the propagation direction was studied experimentally. Mixtures with various concentration gradients were formed by sliding the separation plate which divides a detonation chamber from a diffusion chamber in which a diffusion gas was initially introduced. A stoichiometric hydrogen–oxygen mixture was charged in the detonation chamber, while oxygen or nitrogen was filled in the diffusion gas chamber. Temporal concentration measurement was conducted by the infrared absorption method using ethane as alternate of oxygen. Smoked foil records show a deformation of regular diamond cells to parallelogram ones, which well corresponds to local mixture concentration. Schlieren photographs reveal the tilted wave front whose angle is consistent with the deflection angle of the detonation front obtained from trajectories of the triple point. The local deflection angle increases with increase in local concentration gradient. Calculation of wave trajectory based on the ray tracing theory predicts formation of the tilted wave front from an initial planar front.

Keywords Detonation · Cellular structure · Concentration gradient

PACS 47.40.-x · 47.40.Nm · 47.70.Fw · 82.40.-g · 82.40.Fp

Communicated by Z. Jiang.

K. Ishii (✉) · M. Kojima
Department of Mechanical Engineering,
Yokohama National University,
79-5 Tokiwadai, Hodogaya-ku,
Yokohama 240-8501, Japan
e-mail: kazishii@ynu.ac.jp

1 Introduction

To study detonation propagation in non-uniform mixtures is practically important for safety reasons, since accidental explosions are possible to occur in mixtures in which fuel and oxidizer are not completely premixed. As for onset of detonation in non-uniform mixtures Zel'dovich et al. showed three regimes of possible development of chemical reactions for mixtures with initially non-uniform temperature [1]. Later they studied the problem of evolution of a binary mixture with non-uniform initial distribution of one component [2]. Effects of a non-uniform geometry on detonation initiation were investigated by the multi-dimensional numerical simulations [3]. Sochet et al. made the experimental work concerning detonation initiation in mixtures with non-uniform concentration by rupturing a soap bubble in which a uniform mixture is initially charged [4]. Transmission of detonation from one mixture to the other through an area of continuously changing concentration was experimentally studied using circular detonation tubes [5,6]. These studies revealed the behavior of detonation in mixtures with concentration gradients parallel to the propagation direction. Detonation re-initiation across a non-reactive mixture was studied with reference to critical concentration gradients [7,8]. Detonation traveling in mixtures composed of two-layered medium with different concentrations is referred to layer detonation and its propagation mechanism has been investigated experimentally [9,10] and numerically [11]. Recently several studies have been made to clarify the mechanism of propagation of detonation waves traveling in mixtures with concentration gradient normal to the propagation direction [12,13]. For application to high speed combustors, detonations propagating along concentration gradients have been numerically simulated with reference to stability of combustion in high speed flow [14].

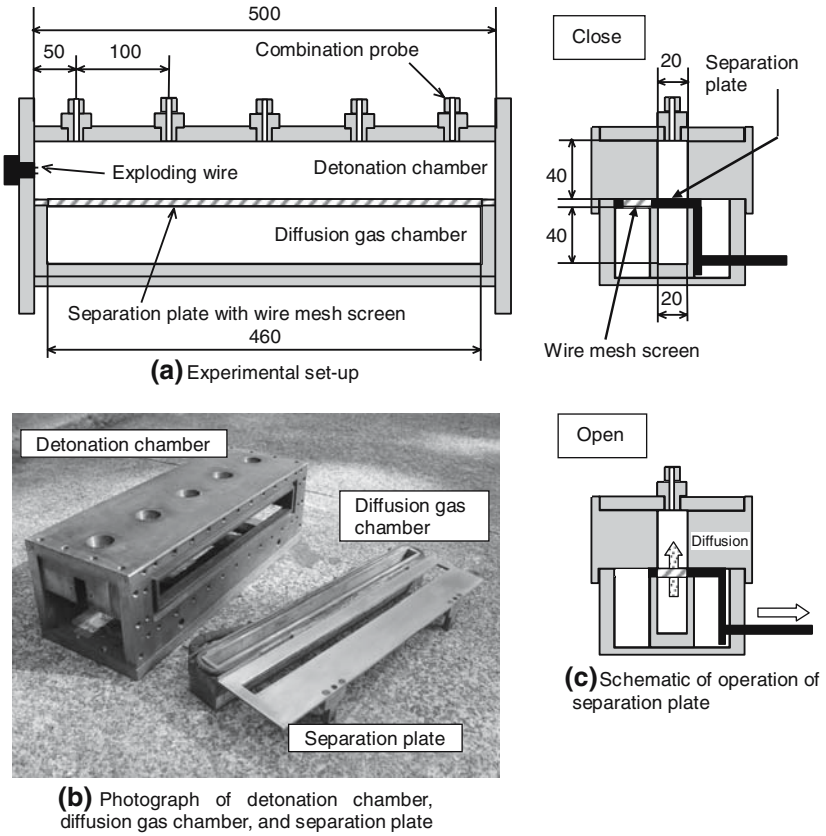

Fig. 1 Schematics of the experimental set-up for formation of mixtures with concentration gradients, dimensions in mm. **a**, **b**, **c**

In the present work detonation propagation in mixtures with continuous concentration gradients whose direction is normal to the propagation direction have been studied experimentally. Attention was paid on the shape of the wave front and triple points trajectory. Using measured distributions of mixture concentration, the calculation of wave propagation has been conducted based on the ray tracing theory.

2 Experimental apparatus

2.1 Detonation chamber

The detonation chamber used in the present work is shown in Fig. 1. It has a rectangular cross-section of 40 mm × 20 mm and its total length is 500 mm. The diffusion gas chamber is attached to the detonation chamber and is initially isolated from it by a separation plate of 5 mm in thickness. This separation plate can be moved by two linear electric motors so that a gas in the diffusion gas chamber can be diffused into the detonation chamber and then a mixture with a concentration gradient is formed. To minimize flow disturbances caused by the motion of the separation plate, a wire mesh screen whose blockage ratio was 0.5 was inserted between the detonation chamber and the diffusion gas chamber. The sidewalls of the detonation chamber can be replaced with windows made of Plexiglas to take schlieren photographs of the detonation propagation.

After the separation plate is fully opened, the mixture filled in the detonation chamber is ignited and a deflagration wave initially travels downstream. Then after the DDT process a detonation wave is initiated and propagates in the mixture with a concentration gradient whose direction is normal to the propagation direction. For fast initiation of detonation, an exploding wire with a maximum stored energy of 2.3 J was used as an ignition source.

To detect a shock and a reaction front individually at one measuring location, five combination probes [15] which consist of a pressure and an ion probe were placed every 100 mm on the upper wall of the detonation chamber. A smoked aluminum foil of 0.2 mm in thickness was fixed to the sidewall to record a variation of the cellular structure. A stoichiometric hydrogen–oxygen mixture was initially charged in the detonation chamber as a test gas and nitrogen or oxygen was filled in the diffusion gas chamber. Initial pressure and initial temperature were 0.1 MPa and ambient temperature, respectively, both in the detonation chamber and the diffusion gas chamber.

2.2 Concentration measurement

Concentration measurement was done by the infrared absorption method. Since most of hydrocarbon fuels absorb infrared light of about 3.4 μm in wavelength, ethane, whose diffusion coefficient is close to that of oxygen, was used as an absorptive gas and mixed with hydrogen as alternate of oxygen. Figure 2 shows a schematic of the optical system for concentration measurement. The infrared light emitted from a blackbody furnace is collimated by a BaF_2 lens and then enters into the detonation chamber through a CaF_2 window fixed to the side wall. The intensity of the transmitted infrared light of about 3.4 μm in wavelength is detected with combination of a thermographic camera (Avionics, TVS-8502) and an interference filter ($\lambda_0 = 3.4$ μm, FWHM = 140 nm). The thermographic camera has a two-dimensional image sensor with high sensitivity for 3.5–4.1 μm and 4.5–5.1 μm in wavelength. Although 3.4 μm is out of the sensitive wavelength according to the specification sheet of the thermographic camera, it was possible to obtain thermographic images. This is probably due to a spectral property of the band-pass filter installed in the thermographic camera.

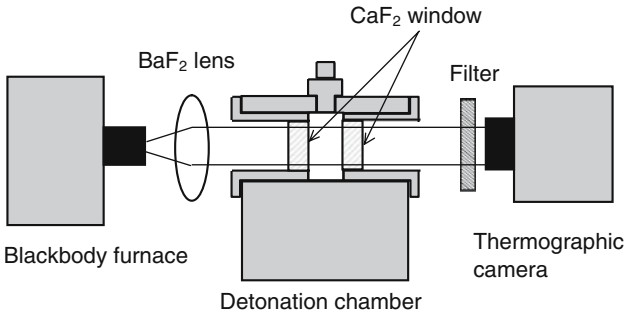

Fig. 2 Optical system of concentration measurement based on the infrared absorption method using a thermography

In absorption methods concentration is usually calculated from a ratio of intensity of transmitted light to incident light using the Lambert–Beer's law. However, the thermographic camera gives an image of the temperature distribution from intensity of the detected infrared light. It is therefore necessary to convert the thermographic image into concentration distribution. In the present work, calibration was conducted using homogeneous hydrogen–ethane mixtures with various mixture ratios to obtain a calibration table relating the temperature signal to a known ethane concentration as reference.

3 Results

3.1 Concentration distribution

Figure 3 shows estimated oxygen concentrations in the detonation chamber in the case that oxygen or nitrogen was diffused into a stoichiometric hydrogen–oxygen mixture. Although the steepest concentration gradient was obtained for a diffusion time $\tau = 5$ s in Fig. 3a, the oxygen concentration at the height of 3 mm from the separation plate shows almost the same value for $\tau = 5$–20 s. As compared to results of a simple calculation on molecular binary diffusion, nitrogen is diffused more rapidly in Fig. 3a, in particular for $\tau = 5$–20 s. This is mainly because of flow disturbances, which were generated by the movement of the separation plate, enhancing the diffusion process near the separation plate. As mentioned in the previous section, for suppression of the flow disturbance, the wire mesh screen was inserted between the detonation chamber and the diffusion gas chamber. From the fact that concentration measurements without the wire mesh screen had resulted in less monotonical concentration distributions with poor repeatability, insertion of the wire mesh screen was effective to minimize the flow

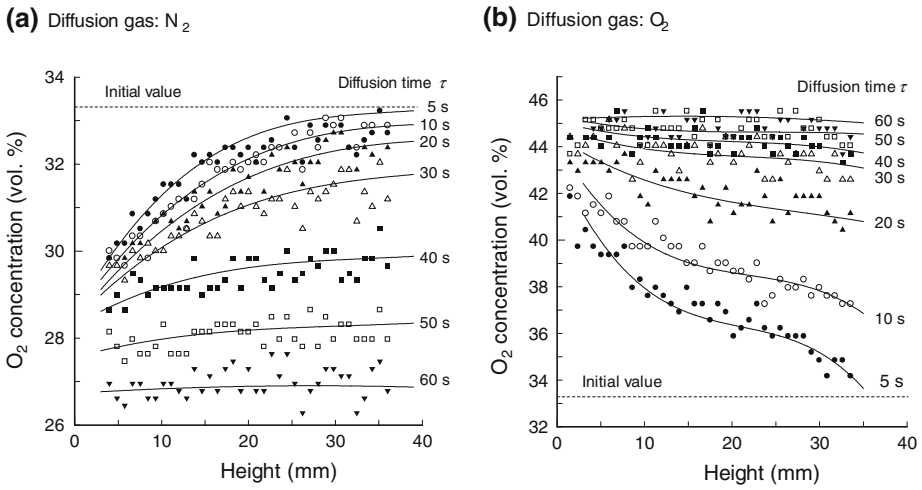

Fig. 3 Estimated concentration of oxygen in the detonation chamber for various diffusion time τ

disturbance, although it could be not totally removed. From several tests under the same experimental condition, it was confirmed that the estimated concentration profiles had a good repeatability.

3.2 Propagation velocity

Figure 4 shows velocities of a shock and a reaction front measured at the upper wall of the detonation chamber with and without diffusion of nitrogen. In Fig. 4a "no diffusion" means that a stoichiometric hydrogen–oxygen mixture is also charged in the diffusion gas chamber so that no diffusion occurs after opening of the separation plate. It is found that a steady detonation is established at a distance of 200 mm from the ignition point. In Fig. 4b steady propagation of detonation is still achieved, whereas increase of diffusion time leads to a slower initiation of the detonation as shown in Fig. 4c. Further increase of diffusion time results in no initiation of detonation. In Fig. 4 V_{CJ} denotes the Chapman–Jouguet velocity at the upper wall calculated from the measured oxygen concentration at the height of 40 mm on the assumption that the equivalence ratio is kept constant of unity during the diffusion process. V_{CJ} is obviously higher than the measured velocity in Fig. 4b and c and this discrepancy is unknown at the present. One explanation may be that the assumption of constant equivalence ratio does not hold for diffusion of nitrogen due to high diffusivity of hydrogen as compared to oxygen. As for diffusion of oxygen, detonation initiation was confirmed in all the test conditions. In these cases the propagation velocity almost agrees with the Chapman–Jouguet velocity calculated from the measured mixture concentration near the upper wall of the detonation chamber.

3.3 Schlieren photograph

Figure 5 shows a typical schlieren photograph for nitrogen diffusion with $\tau = 5$ s, where several images taken at different locations in different tests were superimposed. Since the background of the schlieren images suffer from an inequable density of the Plexiglas, a sketch of the wave fronts is also shown for better understanding. In the schlieren image a shock or a compression wave propagating from left to right is visualized as a black line. The curved white line at a distance of 120 mm indicates a flame front just prior to onset

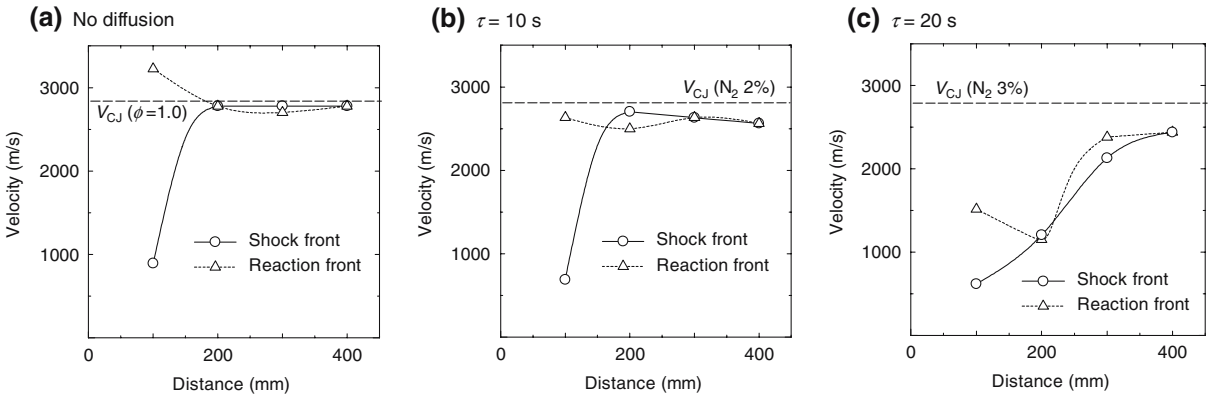

Fig. 4 Velocity profiles of a shock and a reaction front with and without diffusion of nitrogen. Nitrogen concentrations of 2 and 3% in (**b**) and (**c**) were calculated from the measured oxygen concentration at the height of 40 mm on the assumption that the equivalence ratio is kept constant of unity during the diffusion process

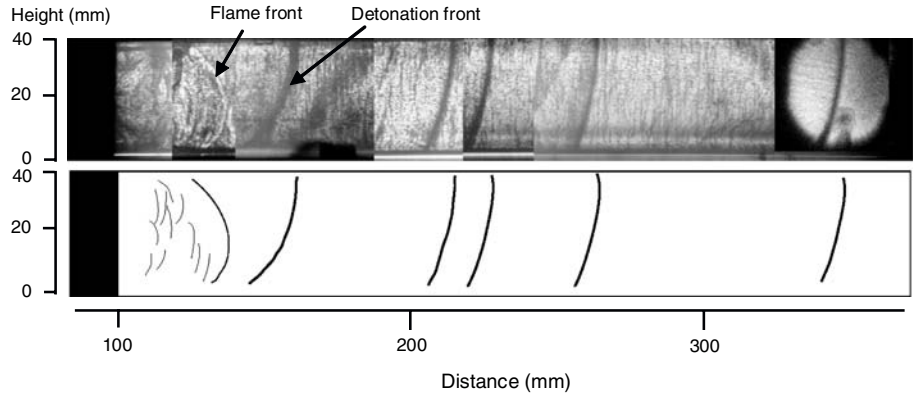

Fig. 5 Typical schlieren photographs showing formation of detonation wave front for nitrogen diffusion. The diffusion time τ is 5 s

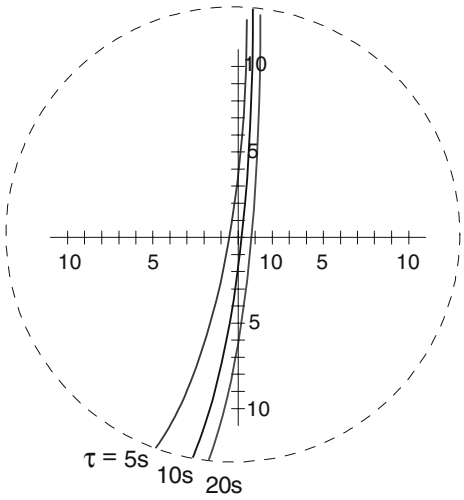

Fig. 6 Sketches of detonation wave front obtained from schlieren photographs for various concentration gradients. The diffusion gas is nitrogen

of detonation and then the tilted wave front of detonation is shown at a distance of 150 mm. At this location the tilt angle of the local detonation front is larger than 40° near the separation plate. As the wave travels, the tilt angle decreases and a steady wave front is achieved at a distance of 200 mm. Figure 6 shows effects of the concentration gradient on the wave front. The tilt angle decreases with increase in diffusion time, namely due to decrease in the concentration gradient.

3.4 Smoked foil records

A typical smoked foil record for diffusion of nitrogen is shown in Fig. 7. In terms of mixtures diluted with oxygen, less distinct variations in the cellular structure owing to concentration distribution were seen on the smoked foil records, regardless of the diffusion time. However, for mixtures diluted with nitrogen, as shown in Fig. 7, it can be seen that the cell size decreases in the direction to the upper wall of the detonation chamber, which well corresponds to the measured concentration distribution. At the height of 40 mm in Fig. 7, namely at the upper wall, a cell size of about 1 mm is seen, which implies less diffusion of nitrogen. While the cellular structure forms a diamond shape near the upper wall, a parallelogram shape is observed near the separation plate. For quantitative evaluation of the shape of the cellular structure, θ_1 and θ_2 are defined as angle between the propagation direction and trajectory of triple points as shown in Fig. 7. At $\tau = 5$ s, the difference between θ_1 and θ_2 near the upper wall is relatively small, indicating the regular diamond cellular structure. This difference increases, as the shape of the cells is deformed to the parallelogram one. The concentration gradient normal to the propagation direction causes the difference in strength between the transverse wave moving upward and downward. The curved wave front combined with this difference of the transverse waves results in the deformation of a diamond shape of the cell to the parallelogram one.

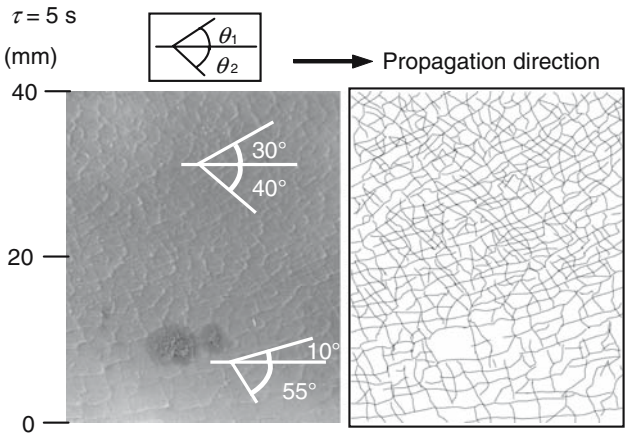

Fig. 7 Smoked foil record for diffusion of nitrogen, $\tau = 5$ s. Image area is 40 mm × 30 mm

4 Discussion

From the previous section it was found that the shape of the detonation front is affected by non-uniformity of the mixture concentration. In the present work the formation of the wave front is calculated using the ray tracing theory [16].

4.1 Ray tracing equations

The velocity of a moving point $\boldsymbol{x}_\mathrm{p}$ which lies on the wave front $t = \tau(\boldsymbol{x}_\mathrm{p})$ is given as

$$\frac{d\boldsymbol{x}_\mathrm{p}}{dt} = c\boldsymbol{n} + \boldsymbol{v}, \tag{1}$$

where c, $\boldsymbol{n}$, $\boldsymbol{v}$ denote a wave speed, a unit vector normal to the wave front, and a velocity vector of the ambient medium. Generally the direction of $\boldsymbol{n}$ changes during wave propagation, an additional equation is needed to calculate an actual wave trajectory. Instead of dealing with $\boldsymbol{n}$ directly, a wave slowness vector $\boldsymbol{s}(\boldsymbol{x}_\mathrm{p}) = \nabla\tau(\boldsymbol{x}_\mathrm{p})$ [16] which is parallel to $\boldsymbol{n}$ can be introduced by the following equation

$$\boldsymbol{s} = \frac{1}{c + \boldsymbol{v}\cdot\boldsymbol{n}}\boldsymbol{n}. \tag{2}$$

Then Eq. (1) is rewritten as

$$\frac{d\boldsymbol{x}_\mathrm{p}}{dt} = c(c + \boldsymbol{v}\cdot\boldsymbol{n})\boldsymbol{s} + \boldsymbol{v}. \tag{3}$$

A differential equation for the time rate of change of $\boldsymbol{s}$ along a wave trajectory can be given as

$$\frac{d\boldsymbol{s}}{dt} = -\frac{1}{c + \boldsymbol{v}\cdot\boldsymbol{n}}\nabla c - \boldsymbol{s}\times(\nabla\times\boldsymbol{s}) - (\boldsymbol{s}\cdot\nabla)\boldsymbol{v}. \tag{4}$$

Equations (3) and (4) are referred to as "ray-tracing equations" with which a wave trajectory can be calculated from initial values of $\boldsymbol{x}_\mathrm{p}$ and $\boldsymbol{s}$ under the condition that temporal and spatial distributions of c and $\boldsymbol{v}$ are known.

In the present work, the ambient gas velocity is zero and the wave speed, namely local Chapman–Jouguet speed V_CJ, can be treated as independent of time, since a characteristic time of gaseous diffusion process is much longer than the propagation time of the detonation in the chamber. By substituting V_CJ for c, Eqs. (3) and (4) reduce to

$$\frac{d\boldsymbol{x}_\mathrm{p}}{dt} = V_\mathrm{CJ}^2\boldsymbol{s}, \tag{5}$$

$$\frac{d\boldsymbol{s}}{dt} = -\frac{1}{V_\mathrm{CJ}}\nabla V_\mathrm{CJ}, \tag{6}$$

Integration of Eqs. (5) and (6) gives the location of a point lying in the initial wave front of a detonation at any instance of time without requiring any information concerning the trajectory of a neighboring point. In the present work, local V_CJ was calculated from the measured concentration distribution and was assumed to be constant in the horizontal direction of the detonation chamber.

4.2 Formation of wave front

Figure 8 shows calculated snapshots of the wave front at several instances for diffusion of nitrogen of $\tau = 5$ s. The formation of a tilted wave front from an initial planar one is well demonstrated in Fig. 8. Dashed-lines indicating the wave trajectory trends in the bottom direction, which is due to the lower wave speed at smaller heights, and are in agreement with the experimental fact that the triple points constructing

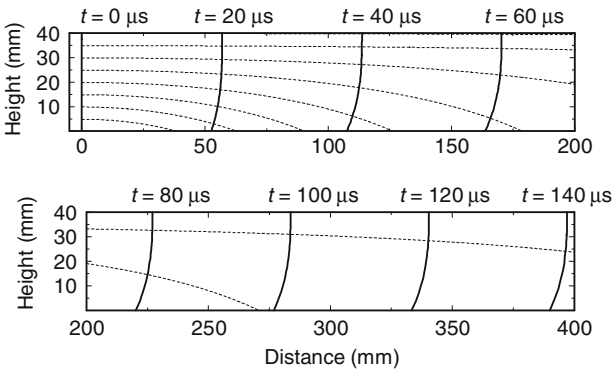

Fig. 8 Calculated wave trajectories from an initially planar wave front corresponding to diffusion of nitrogen, $\tau = 5$ s

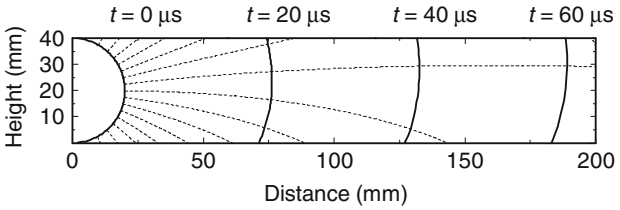

Fig. 9 Calculated wave trajectory from an initially semispherical wave front corresponding to diffusion of nitrogen, $\tau = 5$ s

the cellular structure moves downward in particular at the height of 0–20 mm, as shown in Fig. 7. Points lying in the tilted portion of the wave front at $t = 40$ μs originate from the lower part of the initially planar wave front, while sources of most points in the wave front at $t = 140$ μs lie in the initial wave front higher than 30 mm.

Since propagation started from a planar wave front in Fig. 8, a well-developed wave front was obtained even at $t = 40$ μs. However as shown in Fig. 5, detonation has a curved wave front at its onset, thus the initial condition in Fig. 8 is not in agreement with the present experiment. Therefore, a calculation was done for an initially curved wave front. In Fig. 9 a semispherical wave front whose center of curvature lies at the midpoint of the chamber height was initially given at $t = 0$ μs. The subsequent propagation process of the wave front lead to the tilted wave front, although the wave shape at the early stage of propagation is different from the schlieren image in Fig. 5 where the local wave front is normal to the upper-wall. In Fig. 9 some of trajectories tending upward penetrate the upper wall at the height of 40 mm, because reflection of the wave at the wall boundary is not considered in the present calculation. In the experiment reflection of an initially curved detonation at the wall causes higher pressure and temperature regions, resulting in a local overdriven detonation propagating faster than the initial one. Then this process makes the transformation from the curved wave front to the planar one more rapidly near the upper wall.

4.3 Deflection angle

Figure 10 shows deflection angles of the wave front obtained from the schlieren photographs and the calculated results of the wave trajectory, which were plotted as θ_wave and θ_calc, respectively. The deflection angle is defined as the angle between the local propagation direction and the horizontal axis. From the smoked foil record, the deflection angle θ_soot was estimated in the following manner. On the assumption that a local wave front of a detonation moves along a bisector of the angle of $\theta_1 + \theta_2$, the local deflection angle from the horizontal direction θ_soot is calculated by

$$\theta_\mathrm{soot} = \frac{1}{2}(\theta_2 - \theta_1). \tag{7}$$

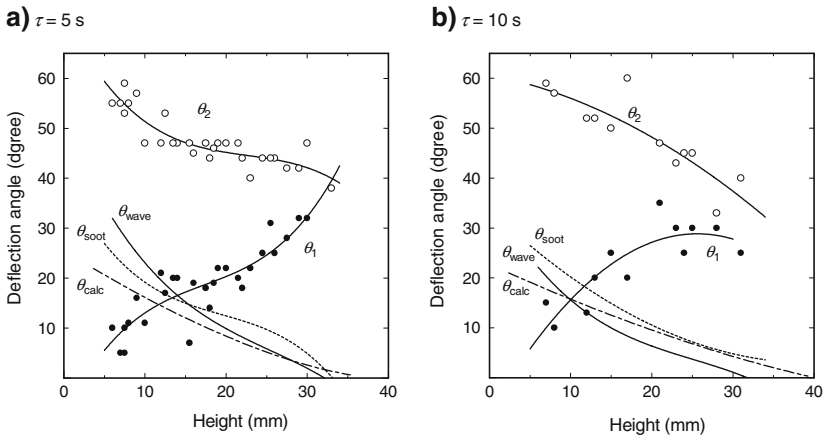

Fig. 10 Deflection angle of wave front obtained from schlieren photographs θ_{wave}, triple point trajectory θ_{soot}, and calculation based on ray tracing theory θ_{calc}. The diffusion gas is nitrogen

θ_{soot} agrees with θ_{wave} within 5° in Fig. 10a and b, which indicates that the triple points trajectories are symmetrical to the direction normal to the local detonation front even in a mixture with concentration gradients. The difference between θ_{calc} and θ_{wave} increases with decrease in the height from the separation plate for $\tau = 5$ s in Fig. 10a, while good agreement between θ_{calc} and θ_{wave} was obtained for $\tau = 10$ s in Fig. 10b. As θ_{calc} is based on the local Chapman–Jouguet velocity calculated from results of concentration measurements, it is deduced that the measured concentration has poor reliability for $\tau = 5$ s. One possible reason for this is refraction of the incident infrared ray in the chamber at the concentration gradient. In the present work the concentration distribution was estimated from infrared absorption using two-dimensional thermographic images. A steep concentration gradient causes larger downward deflection of infrared rays so that apparent large concentration gradients obtained from the thermographic image results in concentration underestimation near the separation plate. In the case of weaker gradients, therefore, a more reliable mixture concentration can be obtained. For further studies some compensation is needed to evaluate a distribution of mixture concentration more accurately.

5 Conclusions

The propagation of detonation waves in mixtures with a concentration gradient whose direction is normal to the propagation direction has been studied experimentally. Concentration measurement was done by an infrared absorption method using ethane as alternate of oxygen. Schlieren photographs reveal the tilted wave front whose deflection angle increases with increase in concentration gradient. Smoked foil records show a deformation of the regular diamond cells to parallelogram ones, which well corresponds to the local mixture concentration. The deflection angle of the detonation front estimated from trajectories of the triple points agrees well with that obtained from schlieren photographs. The calculated wave trajectory based on ray tracing theory predicts the propagation of the detonation front.

Acknowledgments A part of the present work has been supported by MEXT Grant-in-Aid for Young Scientist (B) (KAKENHI 14750721).

References

1. Zel'dovich, Ya.B., Librovich, V.B., Makhviladze, G.M., Sivashinsky, G.I.: On the development of detonation in non-uniformly preheated gas. Astronaut. Acta **15**, 313–321 (1970)
2. Zel'dovich, Ya.B., Gelfand, B.E., Tsyganov, S.A., Frolov, S.M., Polenov, A.N.: Concentration and temperature non-uniformities of combustible mixtures as reason for pressure waves generation. Prog. Astronaut. Aeronaut. **114**, 99–123 (1988)
3. Dorofeev, S.B., Efimenko, A.A., Kochurko, A.S.: Numerical study of detonation self-initiation conditions. In: Proceedings of 15th ICDERS, pp. 425–428 (1995)
4. Sochet, I., Lamy, T., Brossard, J.: Experimental investigation on the detonability of non-uniform mixtures. Shock Waves **10**, 363–376 (2000)
5. Thomas, G.O., Sutton, P., Edwards, D.H.: The behavior of detonation waves at concentration gradients. Combust. Flame **84**, 312–322 (1991)
6. Kuznetsov, M.S., Alkseev, V.I., Dorofeev, S.B., Matsukov, I.D., Boccio, J.L.: Detonation propagation, decay, and reinitiation in nonuniform gaseous mixtures. Proc. Combust. Inst. **27**, 2241–2247 (1998)
7. Bjerketvedt, D., Sonju, O.K., Moen, I.O.: Prog. Astronaut. Aeronaut. **106**, 109–130 (1986)
8. Teodorczyk, A., Thomas, G.O., Ward, S.M.: Transmission of a detonation across an air gap. In: Proceedings of 20th International Symposium Shock Waves, pp. 1095–1100 (1996)
9. Liu, J.C., Liou, J.J., Sichel, M., Kaufmann, C.W., Nichols, J.A.: Diffraction and transmission of a detonation into a bounding explosive layer. Proc. Combust. Inst. **21**, 1639–1647 (1986)
10. Tonello, N.A., Sichel, M., Kauffman, C.W.: Mechanisms of detonation transmission in layered H_2-O_2 mixtures. Shock Waves **5**, 225–238 (1995)
11. Oran, E.S., Jones, D.A., Sichel, M.: Numerical simulation of detonation transmission. Proc. R. Soc. Lond. A **436**, 267–297 (1992)

12. Ishii, K., Takahashi, Y., Tsuboi, T.: Detonation propagation in hydrogen–oxygen mixtures with concentration gradients. In: Proceedings of 18th ICDERS, Paper No. 153 (2001)
13. Ishii, K., Kojima, M.: Propagation of detonation in mixtures with concentration gradients. In: Roy, G., Frolov, S., Shepherd, J. (eds.) Application of Detonation to Propulsion, pp. 32–37. Torus Press, Moscow (2004)
14. Calhoon, W.H.Jr., Sinha, N.: Detonation wave propagation in concentration gradients. AIAA-2005-1167 (2005)
15. Ishii, K., Grönig, H.: Behavior of detonation waves at low pressures. Shock Waves **8**, 55–61 (1998)
16. Pierce, A.D.: Acoustics: an introduction to its physical principles and applications. The Acoustic Society of America (1989)